ACS OMEGA

http://pubs.acs.org/journal/acsodf

Article

Zinc Oleate Nanorod-Induced Vertical Alignment of Nematic Liquid Crystal

Shweta Mishra, Manjuladevi V,* and Raj Kumar Gupta

Cite This: *ACS Omega* 2022, 7, 46466−46474

Read Online

ACCESS | Metrics & More | Article Recommendations | Supporting Information

ABSTRACT: Nanocomposite zinc oxide nanorods capped with oleic acid (ZOR) with positive dielectric anisotropy liquid crystal (LC) 4′-octyl-4-biphenylcarbonitrile (8CB) filled in unaligned cells exhibit homeotropic alignment of host LC molecules. Further, systematic investigation of the textural, dielectric, and conductivity properties of nanocomposites filled in planar cells is performed with increasing concentration of nanorods. At a nanorod concentration ≤0.2 wt % in 8CB, the order parameter of nanocomposite samples is found to be increasing and ionic conductivity is found to be decreasing as compared to pure LC. Beyond 0.3 wt % concentration of nanorods in 8CB, vertical alignment (VA) of host LC is observed even in a planar aligned cell. The VA of LC molecules in ZOR nanocomposites is confirmed through attenuated total reflection−Fourier transform infrared absorption spectra studies.

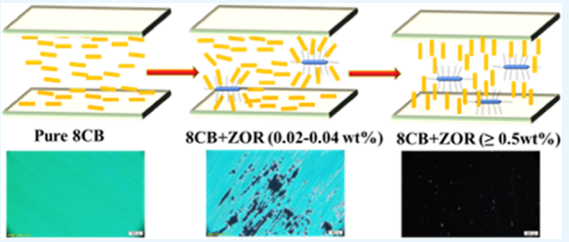

1. INTRODUCTION

Vertical alignment (VA) mode has been adopted for a variety of displays to improve the display performance persistently. This technique fetched revolutionary changes in the field of liquid crystal displays (LCDs). Various alignment modes, viz., planar, twisted nematic,[1,2] VA,[3] in-plane switching (IPS),[4] and fringe-field switching (FFS),[5] are used in LC cells employed for LCDs. In the LC cells, twist, vertical, and splay alignments of the LC molecules are formed in the off-state of the applied field depending on the geometry of the LC cells. Generally, layers of polyimides or silanes with different chemical structures are used to produce such alignments. The main-chain type polyimides are used in the IPS-mode cell to form a homogeneous alignment,[6−8] and silanes or side-chain type polyimides are used in the VA-mode cell to form a homeotropic alignment.[4,9,10] The preparation of these alignment layers usually requires large quantities of solvent, high-temperature operation for the thermal imidization reaction, and a rubbing process. Rubbing process has some serious disadvantages like debris creation, electrostatic discharge, and partial particles which can introduce local defects and streaks and result in low-quality LCDs.[11] In comparison to FFS and IPS modes, the VA mode does not include any rubbing process for device fabrication and offers a very high contrast at normal incidence, mainly attributed to the initial VA of LCs.[3] The LC cells prepared without using alignment layers are suitable for fabricating flexible LC displays which require a low-temperature process.[12] Dispersion of nanoparticles (NPs) shows a promising and easier approach for VA instead of using processes like self-assembled monolayers, photoalignment, or evaporated oxide.[13−15] Several groups have reported VA of LCs using different NPs such as fullerenes,[16] gold NPs,[17,18] nickel NPs,[19] quantum dots,[20,21] and polyhedral oligomeric silsesquioxane (POSS) NPs.[13,16,22,23] These VALC devices without any alignment layer displayed an ideal dark state under crossed polarizers. The realization of true dark state without application of external field helps to produce a high contrast ratio in LCDs. Apart from displays, VALC devices find applications in sensors as well.[24,25] Nakamura et al. proposed that VA can be induced by using fullerene particles without using alignment layers.[26] Jeng et al. reported VA of the LCs without an alignment layer by addition of NPs of POSS into negative dielectric anisotropy LCs.[16,23,27] The electro-optical properties of these LC cells were found to be similar to a conventional homeotropic LC cell with alignment layers. The major problems for the application of POSS are poor compatibility with LC media and weak interaction with LC molecules.[28] Pristine POSS NPs highly aggregate themselves in the LC media and create macroscopic micron size domains resulting in severe light scatterings.[22,29] Addition of 1D nanomaterials to LC hosts in small quantities has shown betterment of the display parameters such as electro-optic switching time, contrast ratio, and threshold voltage as observed by various research groups.[30−33] Addition of various types of carbon nanotubes is widely studied and proven to show great potential as a doping material in LC for device

Received: August 13, 2022
Accepted: November 21, 2022
Published: December 5, 2022

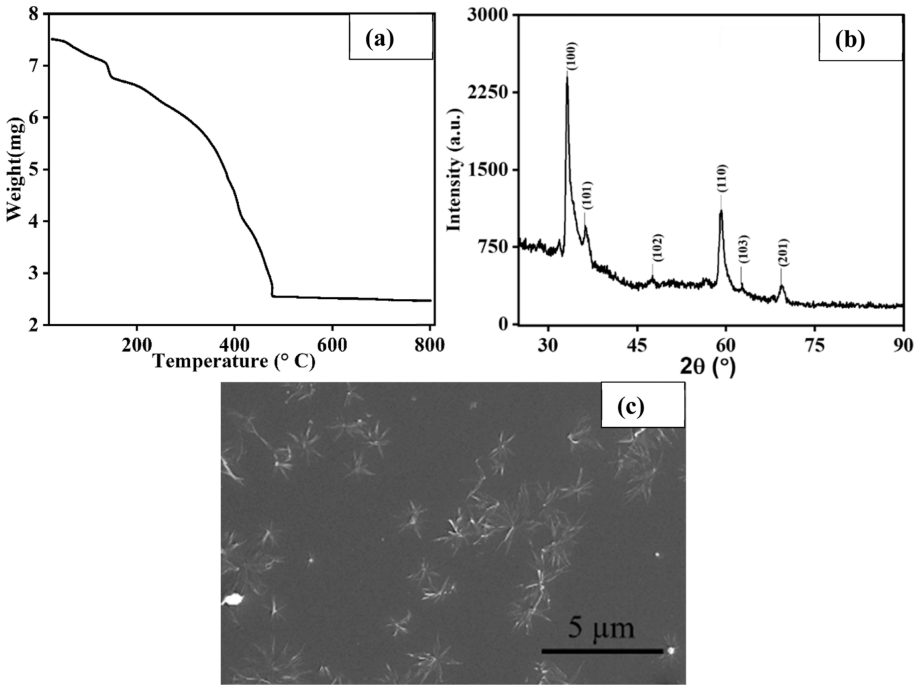

Figure 1. (a) TGA curve during heating cycle under N_2 flow, (b) powder XRD pattern, and (c) FE-SEM image of synthesized ZOR.

applications.[34−36] However, VA with the addition of 1D nanomaterials is yet to be explored. Here, we present the alignment properties of host LC molecules with positive dielectric anisotropy by addition of zinc oxide nanorods capped with oleic acid (ZOR). The vertically aligned domains of LC molecules are observed in unaligned LC cells with addition of a low amount (0.3−0.5 wt %) of ZOR. Systematic investigation of the effect of concentration of ZOR on the dielectric and conductivity properties of host LC and its nanocomposites filled in planar cells is performed. The homeotropic alignment of LC molecules is observed despite the presence of a homogeneous alignment layer. The results are compared with the measurement carried out on nanocomposites filled in conventional homeotropic cells.

2. EXPERIMENTAL SECTION

2.1. Synthesis of ZOR. ZOR are synthesized using the reflux method.[37] Zinc acetate dihydrate [$Zn(OAc)_2$], trioctylamine, and oleic acid are purchased from Sigma-Aldrich and used as received. In a typical synthesis procedure, 4 mmol $Zn(OAc)_2$ is added to 12 mmol oleic acid followed by addition of 7.5 mL of trioctylamine under constant stirring. The reaction is carried out at 280 °C for 2 h. The color of the solution gradually changes to yellow and becomes little cloudy indicating the formation of nanorods. After the completion of reaction, the solution is cooled down to room temperature and washed using ethanol several times until all unreacted solvent is removed. The final product is dried in air at 80 °C and preserved for further studies.

Thermogravimetric analysis (TGA; PerkinElmer TGA4000) of the prepared sample is shown in Figure 1a. The actual weight loss is observed from 250 to 480 °C which shows the formation of ZOR.[38] The powder X-ray diffraction (XRD) pattern of synthesized ZOR was obtained using a Rigaku SmartLab Studio II diffractometer. Field emission scanning electron microscopy (FE-SEM) image of ZOR is captured using a FEI Apreo LoVac instrument. Figure 1b shows the XRD pattern of as-synthesized ZOR. The morphological structure of the synthesized ZOR is shown in Figure 1c. The nanorods obtained are bunched together to form a flowerlike structure. As observed from the FE-SEM image, the nanorods are 50−60 nm wide and 1−1.2 μm in length.

2.2. Preparation of LC Sample Cells. For this experimental study, we have taken 4′-octyl-4-biphenylcarbonitrile (8CB) as the liquid crystalline host material procured from Sigma-Aldrich. The phase sequence of LC host 8CB is as follows: I (40.5 °C) N (32.5 °C) SmA (21.5 °C) Cr.

The solution of 0.25 mg/mL of ZOR in chloroform is prepared and is ultrasonicated for about 2 h to get a homogeneous dispersion. Calculated quantity of this solution is added into host LC to obtain various nanocomposites of concentrations (C_{ZOR}), viz., 0.05, 0.1, 0.2, 0.3, 0.4, 0.5, 1, and 2 wt % of ZOR in 8CB. Sufficient time is allowed for the solvent to evaporate from the nanocomposites. For the electro-optic and dielectric measurements, we have used planar aligned cells of thickness ∼7.5 μm. Planar cells are prepared by spin coating a layer of polyimide (PI2555) on top of the indium tin oxide (ITO)-coated glass plates and cured at 250 °C for about an hour. These PI-coated substrates are further unidirectionally rubbed using a soft cloth, and planar cells are prepared by placing these plates with the rubbing direction antiparallel to each other. Homeotropic cells are also prepared using ITO plates treated with octadecyltrimethylsilane and cured at 100 °C. Cells in both planar as well as homeotropic alignments are prepared by using epoxy glue mixed with glass spacers.

2.3. Characterization Techniques. Thickness of the sample cells is measured using an interferometric fiber-optics spectrometer (Ocean-optics USB4000-XR1-ES). To study the alignment characteristics, cells using ITO plates with no alignment layers (unaligned cells) are also prepared. Optical texture of the LC filled sample cells is observed under a polarizing optical microscope (POM; Olympus BX53M) at room temperature. The sample cell is placed inside the hot stage (Micro-optik MDTC600) with temperature control of

https://doi.org/10.1021/acsomega.2c05196
ACS Omega 2022, 7, 46466−46474

0.1 °C having a small hole in the middle to allow light to pass through. This assembly was then kept on the rotating stage of the POM between crossed polarizers. A laser beam of wavelength 633 nm passes through the sample placed between crossed polarizers. The planar cell is kept between crossed polarizers with the rubbing direction at an angle of 45° to either of the polarizers. The transmitted intensity (I_{tr}) as a function of temperature is recorded and used to estimate the birefringence (Δn) of the samples. As added NPs do fluoresce, fluorescence confocal microscopy (FCM) (ZEISS LSM880) with laser of wavelength λ = 370 nm is performed to investigate the bulk and interfacial properties of ZOR in the host LC. Dielectric permittivity (ε) measurements as a function of voltage are performed at an applied frequency of 4 kHz. Dielectric permittivity at an applied voltage less than the threshold voltage ($\varepsilon_{low(p)}$) and larger than the threshold voltage ($\varepsilon_{high(p)}$) is measured using planar cells filled with pure and ZOR nanocomposites of 8CB. Threshold voltage (V_{th}) is measured with the help of the capacitance−voltage ($C-V$) curve for nanocomposite samples filled in the planar cell. Simultaneous measurements of components of conductivity, $\sigma_{high(p)}$ and $\sigma_{low(p)}$, are also performed using the method reported earlier.[10] Measurement of dielectric permittivity is also performed by application of electric field to homeotropic cells (ε_h) filled with pure as well as ZOR-doped 8CB. All measurements were recorded through a PC with the help of LABVIEW program. To understand the role of ZOR in the VA of 8CB, Fourier transform infrared (FTIR) absorption spectra of films of pure and ZOR-doped 8CB in the attenuated total reflection (ATR) mode were obtained using a PerkinElmer spectrophotometer equipped with GladiATR. The ATR substrate is made up of diamond crystal with an incident angle of 45°. The sample-filled planar cell is broken laterally to acquire the ATR−FTIR spectra of aligned sample films. Similar samples were used to acquire the thin-film XRD pattern to investigate the change in the smectic bilayer structure (SmA_d) of pure 8CB with the addition of ZOR. FTIR and XRD measurements are performed at room temperature where host LC exhibits a smectic phase.

3. RESULTS AND DISCUSSION

The optical textures of pure and ZOR nanocomposites of 8CB observed under cross polarizers of POM are as shown in Figure 2. The POM images of samples filled in the planar cell are shown in the first row of Figure 2, whereas the second and third rows show the optical textures of samples filled in homeotropic and unaligned cells, respectively. The optical textures of pure and 0.2, 0.3, and 2 wt % ZOR nanocomposites of 8CB in the nematic phase (T = 35 °C) are shown here. Detailed POM images are shown in Figure S1 in the Supporting Information. Homogeneous and uniform alignment of molecules of pure LC is observed in planar and homeotropic cells, whereas characteristic schlieren texture of the nematic phase can be observed in uncoated cells as shown in Figure 2a. The addition of ZOR for concentration upto 0.2 wt % (taken as critical concentration, C_{ZOR}*) of 8CB also shows uniform alignment as observed in Figure 2b. When C_{ZOR} increases to 0.3 wt % in 8CB, we can notice the presence of homeotropically aligned domains in the planar cell as observed from Figure 2c (first row). With a further increase in C_{ZOR}, vertically aligned domains increase. Complete dark texture of the planar as well as uncoated cells, similar to that of the homeotropic cells filled with ZOR nanocomposites of 8CB can be observed for $C_{ZOR} \geq 0.5$ wt % on rotation of the microscope stage under crossed polarizers as shown in Figure S1. This shows that the presence of ZOR in 8CB helps the host LC molecules to align vertically owing to the interaction between ZOR and LC molecules. However, no aggregation of ZOR is observed in nanocomposite samples for the samples under investigation. FCM images of pure and ZOR nanocomposites of 8CB are shown in Figure 3. The FCM images (left panel) are split into RGB components, and the blue component (indicating fluorescence of ZOR) is considered for drawing a line profile along the arrows as shown in the FCM images (right panel). Pure 8CB does not show any fluorescence (Figure 3e), and hence its analysis is not presented. However, fluorescence in ZOR nanocomposites of 8CB clearly indicates ZOR uniformly dispersed in the bulk of LC. As it can also be observed from the line profile, the higher value of fluorescence intensity appears in the bulk region of the sample cells filled with nanocomposites having dispersed ZOR (Figure 3b−d). To further comprehend the inference, a sample cell is prepared with the ZOR directly coated on the ITO substrate. This cell is then filled with pure 8CB, and FCM images are recorded. The line profile for this sample (right panel, Figure 3a) shows significant overlap in the interfacial region.

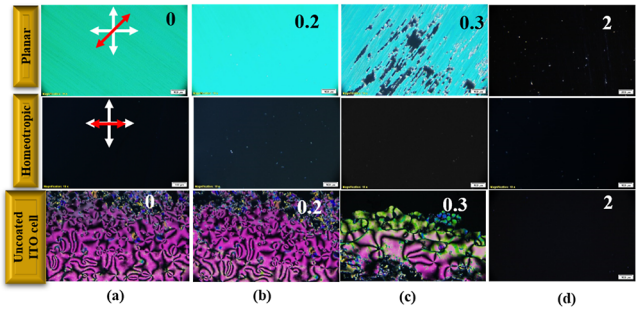

Figure 2. (a−d) Optical textures of pure and ZOR nanocomposites of 8CB (T = 35 °C) in planar cells (row 1), homeotropic cells (row 2), and unaligned cells observed under POM (numbers show C_{ZOR} in 8CB).

The alignment of LC molecules in nanocomposites depends on the shape of the NPs, chemical modification of the surface of particles, the miscibility of particles in the host, and the properties of the confining substrates.[39,40] Several groups have shown that functionalized spherical NPs or quantum dots (4−5 nm) accumulate at the surface of the substrate due to the low miscibility with the nematic hosts altering the boundary conditions which results in the modification of the initial alignment layer.[21,41,42] However, the 1D shape anisotropy similar to that of LC molecules and the large aspect ratio (∼50:1000 nm) of ZOR help LC molecules to form domains around dispersed nanorods. Hence, the presence of ZOR is observed to be in the bulk instead of accumulating at the surface.

Based on the observation of optical textures, birefringence of pure and ZOR nanocomposites of 8CB is performed for $C_{ZOR} < C_{ZOR}$*. The temperature variation of birefringence (Δn) for samples filled in planar cells is shown in Figure 4. The change in the value of Δn is observed to be negligible as compared to the pure LC with the addition of ZOR. The decrease in the value of Δn as a function of temperature is observed at C_{ZOR}* as compared to pure 8CB.

https://doi.org/10.1021/acsomega.2c05196
ACS Omega 2022, 7, 46466−46474

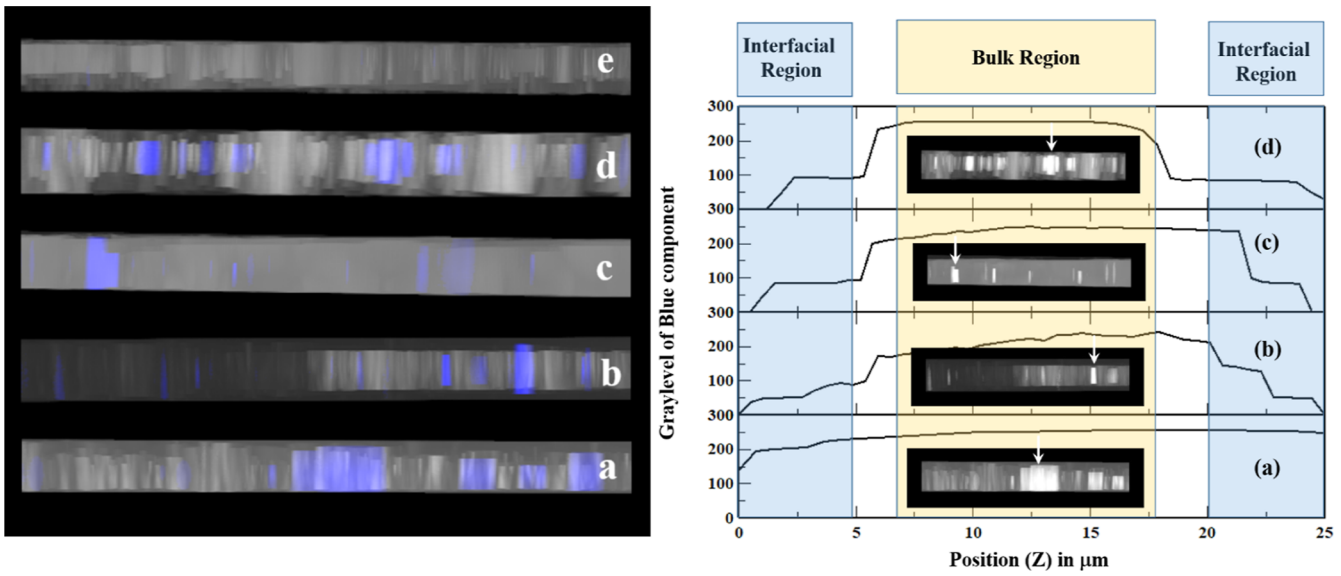

Figure 3. (left panel) FCM images and (right panel) analysis of FCM images of the (a) sample cell prepared by ZOR-coated ITO substrate and then filled with 8CB and (b) 0.05, (c) 0.3, (d) 2 wt % ZOR nanocomposites of 8CB (T = 35 °C) in planar cells. (e) FCM image of pure 8CB showing no fluorescence.

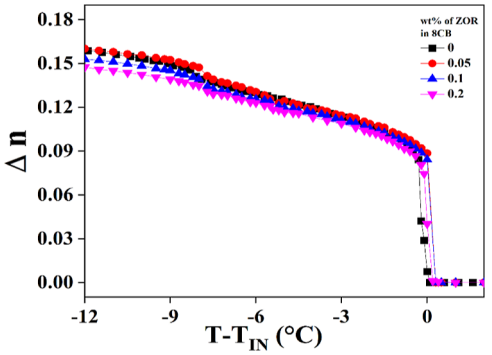

Figure 4. Birefringence (Δn) of pure and ZOR nanocomposites of 8CB ($C_{ZOR} \leq C_{ZOR}$*) as a function of temperature.

Variation of dielectric permittivity as a function of temperature for pure and ZOR nanocomposites of 8CB filled in planar cells is presented in Figure 5. Here, the component of dielectric permittivity measured at V (0.5 V) < Vth is abbreviated as $\varepsilon_{low(p)}$, whereas the one measured at V (5 V) > Vth is abbreviated as $\varepsilon_{high(p)}$. In the isotropic phase, the value of dielectric permittivity ε_{iso} increases with the increase in concentration of ZOR in 8CB probably due to the presence of short-range nematic order in the isotropic phase of nanocomposite samples. At $C_{ZOR} \geq C_{ZOR}$*, the value of ε_{iso} starts decreasing but is still higher than that of pure LC. The value of $\varepsilon_{low(p)}$ increases with increase in the C_{ZOR} in 8CB as shown in Figure 5a. At C_{ZOR}*, a sudden increase in the value $\varepsilon_{low(p)}$ can be observed as shown in Figure 5b. This is because the added ZOR helps the LC molecules in the vicinity of ZOR to orient vertically by overcoming the anchoring energy. The inference is further supported by FTIR and XRD measurements discussed later. The variation of threshold voltage (Vth) as a function of temperature in pure and nanocomposite samples <C_{ZOR}* of nanorods is shown in Figure 5c. The value of Vth in the nematic phase which is proportional to the order parameter of the nematic phase increases with decreasing temperature. However, Vth diverges as we approach the N-SmA transition temperature due to the formation of short-range ordered cybotactic groups in the nematic phase.[43] Variation of Vth as a function of temperature in nanocomposite samples clearly indicates that the nematic phase range has increased for C_{ZOR} = 0.05 wt % which is consistent with the results shown in Figure 5a. With further increase in C_{ZOR} = 0.1 wt %, the temperature range for the nematic phase reduces but is similar to that of pure LC.

The measurement of Vth for $C_{ZOR} \geq$ 0.2 wt % is not possible due to the tendency of VA of LC molecules with the aid of ZOR in nanocomposite samples as observed in Figure 5a. At C_{ZOR} = 0.3 wt %, the value of $\varepsilon_{low(p)}$ as a function of temperature almost flattens due to the coexistence of vertically aligned as well as planar aligned domains as evident from optical textures as well. The measurement of Vth for concentration of ZOR $\geq C_{ZOR}$* is not possible because of the tendency of LC molecules to vertically align in the presence of ZOR. For $C_{ZOR} \geq$ 0.4 wt %, the curvature of $\varepsilon_{low(p)}$ as a function of temperature changes its sign due to the dominance of vertically aligned domains which is clearly evident from the optical textures. Here, the value of $\varepsilon_{low(p)}$ changes similar to the variation of the parallel component of dielectric permittivity. Kumar et al. proposed that adsorption of ZnO NPs on the substrate surface helps to reduce the surface energy of the substrate which subsequently produces the homeotropic alignment.[44] Choudhary et al. reported that the enhanced local ordering of nematic LC molecules on the surface of NPs contributes largely to inducing homeotropic alignment of bulk LC material within the confined geometry of the sample cell.[45] The values of $\varepsilon_{high(p)}$ are observed to be increasing at any given temperature for all ZOR nanocomposites as compared to pure LC as shown in Figure 5a. The increase in the value of $\varepsilon_{high(p)}$ is attributed to the increase in the net dipole moment of the ZOR nanocomposites of 8C and hence the order parameter, as compared to pure LC. Singh et al. reported that the enhancement in the net dipole moment of the nanocomposite system shows a parallel correlation between the dipole moments of LC molecules and nanorods.[46] A sudden decrease in the value of $\varepsilon_{high(p)}$ observed at the N-

https://doi.org/10.1021/acsomega.2c05196
ACS Omega 2022, 7, 46466−46474

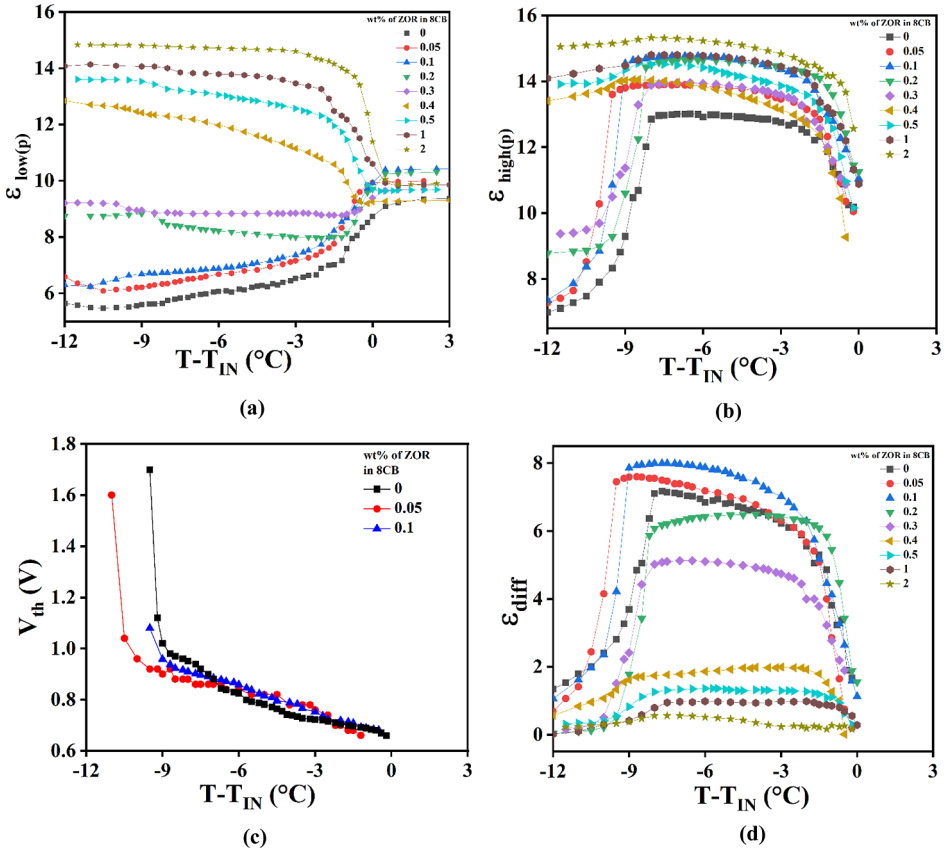

Figure 5. Variation of (a,b) components of dielectric permittivity as a function of temperature, (c) threshold voltage (($C_{ZOR} \leq C_{ZOR}^*$)), and (d) $\varepsilon_{diff} = \varepsilon_{high(p)} - \varepsilon_{low(p)}$ for pure and ZOR nanocomposites of 8CB filled in planar cells as a function of temperature.

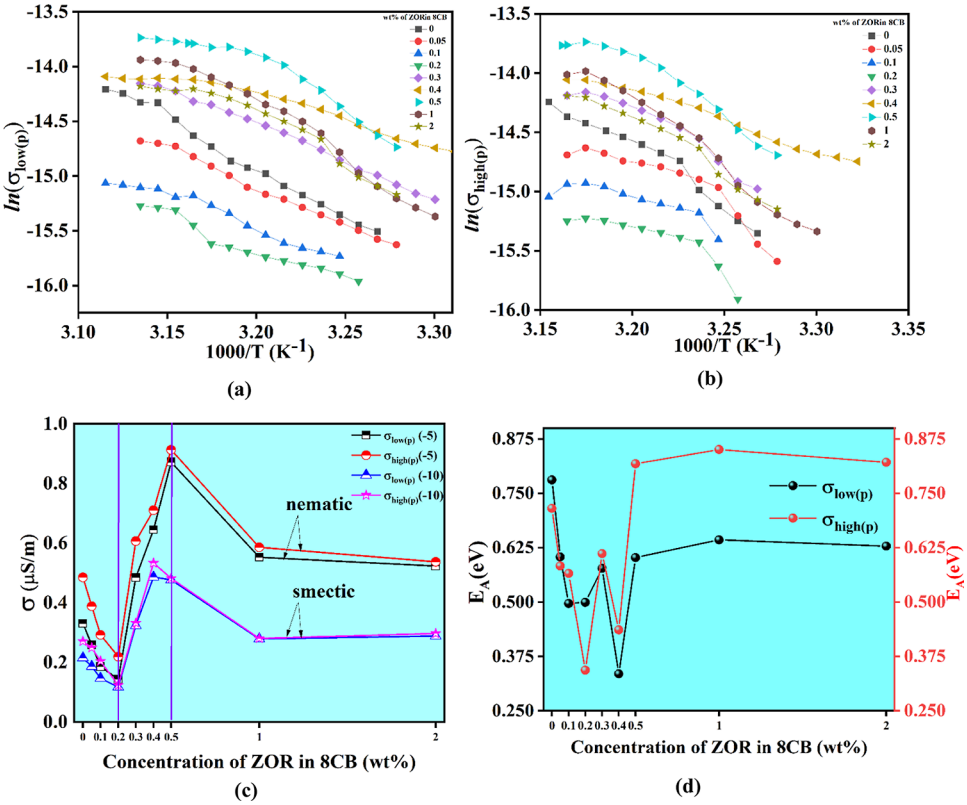

Figure 6. Variation of (a,b) components of bulk ac conductivity as a function of temperature; (c) bulk ac conductivity as a function of C_{ZOR} [numbers in the bracket denote $T - T_{IN}$ (°C)]; (d) thermal activation energy as a function of C_{ZOR}.

https://doi.org/10.1021/acsomega.2c05196
ACS Omega 2022, 7, 46466−46474

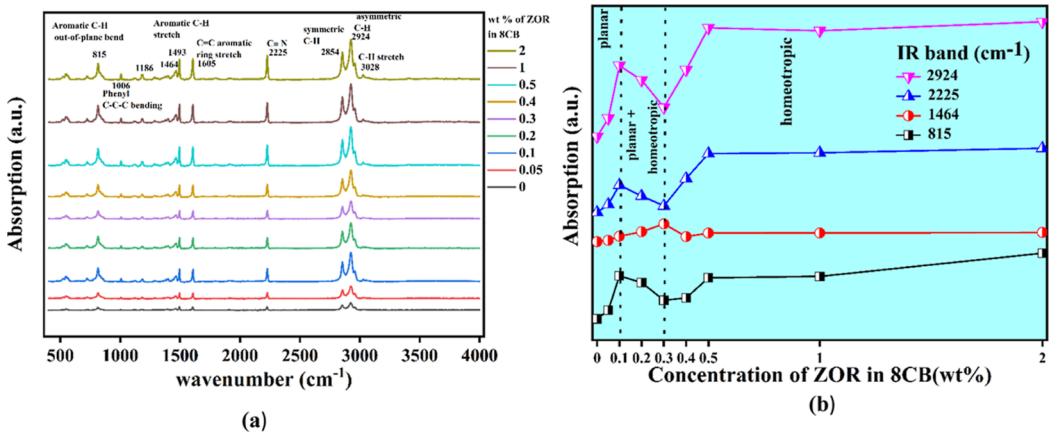

Figure 7. (a)ATR−FTIR absorption spectra and (b) variation of absorption intensity of IR bands as a function of C_{ZOR} of pure and ZOR nanocomposites of 8CB.

SmA transition temperature is due to the negligible effect of applied electric field on the orientation of LC molecules due to emergence of smectic layering. The difference ($\varepsilon_{diff} = \varepsilon_{high(p)} - \varepsilon_{low(p)}$) for pure and ZOR nanocomposites of 8CB is shown in Figure 4d. The initial addition of ZOR ($C_{ZOR} < C_{ZOR}$*), the values of ε_{diff} increase compared to that of pure LC. The nematic temperature range is also observed to increase by 1.5 °C for C_{ZOR} = 0.05 wt % compared to pure 8CB. The value of ε_{diff} as well as the nematic temperature range goes on decreasing with increase in $C_{ZOR} \geq C_{ZOR}$*. The value of ε_{diff} is almost zero for C_{ZOR} = 2 wt % which confirms that alignment of 2 wt % nanocomposite of 8CB is nearly homeotropic in the planar aligned cell. The value of ε_h measured for samples filled in homeotropic cells are compared with the values of $\varepsilon_{high(p)}$ measured using planar aligned cells. The value of $\varepsilon_{high(p)}$ measured for the nanocomposite sample with the lowest concentration C_{ZOR} = 0.05 wt % is ∼5% lower than that of the value of ε_h due to the surface anchoring of LC molecules in the nanocomposite sample filled in the planar cell. With the increase in C_{ZOR}, the value of $\varepsilon_{high(p)}$ approaches the value of ε_h and is in agreement (∼0.5% lower) for C_{ZOR} = 2 wt % which suggests that the nearly homeotropic configuration is achieved even in planar aligned cells.

The components of bulk ac conductivity at 0.5 V ($\sigma_{low(p)}$) and 5 V ($\sigma_{high(p)}$) are also measured for pure and ZOR nanocomposites of 8CB, and the temperature variation of ln (σ) is shown in Figure 6a,b. The interesting fact observed here is that we obtain two regimes, one where bulk conductivity decreases ($C_{ZOR} \leq C_{ZOR}$*) and the other where bulk conductivity is higher than that of pure 8CB ($C_{ZOR} > C_{ZOR}$*). The former one may be considered as the ion-capturing regime where the ionic impurities in the bulk 8CB are adsorbed by the added ZOR.[47] In the latter case, the formation of vertically aligned domains facilitates the mobility of ions along with addition of external ions which causes the increase in conductivity in nanocomposite samples as compared to pure LC. Maximum decrease of 57% in the ionic conductivity of the nanocomposite system for $C_{ZOR} < C_{ZOR}$* is also observed due to adsorption of ionic impurities by ZOR. The variation of σ as a function of C_{ZOR} in 8CB is shown in Figure 6c, which shows that the value of σ becomes almost constant after attaining a maximum at C_{ZOR} = 0.5 wt %. The analysis of temperature dependence of bulk conductivity shows that it can be satisfactorily described by the Arrhenius relationship, $\sigma = \exp\left(-\frac{E_A}{k_\beta T}\right)$, where E_A is the thermal activation energy. The variation of activation energy with increasing concentration of ZOR in 8CB is shown in Figure 6d for both components of bulk ac conductivity. The behavior of bulk conductivity of ZOR nanocomposites of 8CB can be explained using a simple model of thermal activation.[48,49] As observed from Figure 6d, the thermal activation energy becomes almost constant for $C_{ZOR} \geq$ 0.5 wt %, that is, when the host LC molecules are almost vertically aligned in the presence of ZOR.

To understand the role of ZOR in the VA of 8CB molecules, FTIR spectra of pure and ZOR nanocomposites of 8CB are recorded. The ATR−FTIR spectra recorded in the range 400−4000 cm^{-1} of pure and ZOR nanocomposites of 8CB are shown in Figure 7a. The IR band at 1792 cm^{-1} which is assigned to the bridging C═O band is observed in all ZOR nanocomposites and not observed for pure 8CB (Figure 2). The characteristic bands of 8CB are identified,[50] and the integrated absorption for some of the bands as a function of concentration of ZOR in 8CB are shown in Figure 7b. It can be noted from the variation that the integrated absorption increases due to incorporation of ZOR. The absorption of a given band depends on the interaction of the corresponding transition dipole moment and the IR field. In a planar cell filled with pure LC, molecules lie nearly flat to the surface. Therefore, the volume density of the transition dipole moments is expected to be least in this geometry. This gives rise to least absorption for any bands where the molecules are constrained in planar geometry. Similarly, in the homeotropic geometry, the volume density of the transition dipole moment of a given band is expected to be large which gives rise to the highest value for the absorption band. These behaviors are clearly seen from Figure 7b. Due to incorporation of the ZOR, the planar alignment of the molecules gets perturbed and a fraction of molecules show a tendency to align vertically. Due to this perturbed alignment with the increase in C_{ZOR}, an increasing trend in the absorption values is observed. The samples with $C_{ZOR} \geq$ 0.5 show a complete homeotropic alignment. The intermediate concentration ranges 0.2−0.4 wt % of ZOR may indicate the transition wherein both the planar and homeotropic alignments coexisted.

Further, the XRD patterns of pure and ZOR nanocomposites of 8CB are recorded. The peak in the low-angle

https://doi.org/10.1021/acsomega.2c05196
ACS Omega 2022, 7, 46466−46474

region (<6°) as shown in Figure 8 arises due to scattering by the LC molecules. The layer spacing (d) corresponding to 2θ

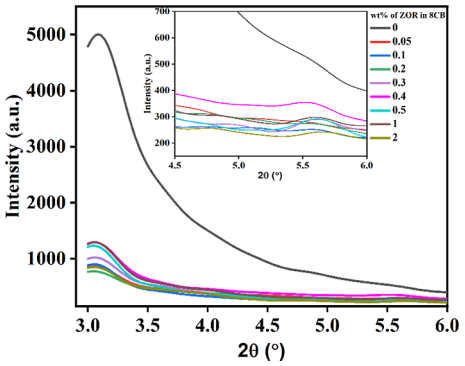

Figure 8. XRD pattern of pure and ZOR nanocomposites of 8CB.

$\sim$ 3.09° is 24.86 Å, which is typical of the partial bilayer structure of pure 8CB in the SmA phase.[51,52] With the increase in the concentration of ZOR, this peak gets broadened. However, the emergence of a new peak at 2θ $\sim$ 5.5° is observed for ZOR nanocomposites of 8CB for $C_{ZOR} \geq C_{ZOR}$* corresponding to the layer spacing of 13.92−13.6 Å which clearly indicates that there is change in the partial bilayer layer spacing of ZOR nanocomposites of 8CB due to the coexistence of homeotropic and planar domains.

A model is proposed based on the observed results as shown in Figure 9 showing the role of ZOR in the VA of host 8CB molecules. The molecular length of oleic acid functional group ($\sim$19.2 Å) is comparable to that of the host 8CB molecule ($\sim$22 Å). Also, the molecules of 8CB can have pretilt angles upto 22° with respect to the substrate surface as reported earlier.[53] When the concentration of ZOR is low in the nanocomposite samples, the nanorods are preferentially near the substrate surface where the anchoring energy of the substrate holds the host LC molecules to exhibit the planar configuration (schlieren texture in case of uncoated cells). With further increase in the concentration of ZOR, the nanorods in the bulk of the system cause the host LC molecules to align vertically achieving homeotropic configuration. The van der Waal's interaction between the oleic acid functional group and the 8CB molecule might help the host LC molecules overcome the anchoring energy of the substrate surface to align in the homeotropic configuration.

4. CONCLUSIONS

ZOR are synthesized using the reflux method. The crystalline phase and morphological structures of the synthesized ZOR are confirmed using powder XRD and FE-SEM measurements. Nanocomposites of positive dielectric anisotropy LC, 8CB, with synthesized ZOR are prepared. Homeotropic alignment of host LC molecules is observed for ZOR concentration above the critical concentration of 0.2 wt % in 8CB. The VA can be achieved in unaligned ITO cells as well, which signifies that interaction of ZOR with host LC is responsible for VA of LC molecules. The nematic temperature range increases in ZOR nanocomposites of 8CB at $C_{ZOR} < C_{ZOR}$* due to an increase in the net dipole moment of the system and hence the order parameter. Maximum decrease of 57% in the ionic conductivity of the nanocomposite system for $C_{ZOR} < C_{ZOR}$* is also observed due to adsorption of ionic impurities by ZOR.

■ ASSOCIATED CONTENT

Supporting Information

The Supporting Information is available free of charge at https://pubs.acs.org/doi/10.1021/acsomega.2c05196.

Detailed POM images for pure and ZOR nanocomposites of PCH5 in planar, homeotropic, and unaligned cells as well as the ATR−FTIR absorption spectra of all samples filled in planar cells showing comparative intensity and low intensity peaks (PDF)

■ AUTHOR INFORMATION

Corresponding Author

Manjuladevi V − *Department of Physics, Birla Institute of Technology and Science (BITS Pilani), Pilani 333031, India;* orcid.org/0000-0002-9358-9453; Email: manjula@pilani.bits-pilani.ac.in

Authors

Shweta Mishra − *Department of Physics, Birla Institute of Technology and Science (BITS Pilani), Pilani 333031, India*

Raj Kumar Gupta − *Department of Physics, Birla Institute of Technology and Science (BITS Pilani), Pilani 333031, India;* orcid.org/0000-0001-5755-1143

Complete contact information is available at: https://pubs.acs.org/10.1021/acsomega.2c05196

Notes

The authors declare no competing financial interest.

■ ACKNOWLEDGMENTS

The authors S.M. and M.V. gratefully acknowledge the DST, SERB for the support provided under the project number EMR/2016/005782 and the BITS Pilani. We thank the Department of Physics, BITS Pilani, Pilani Campus for providing the XRD facility created with the support from DST-FIST (no. SR/FST/PS-I/2017/30). We also thank the Department of Chemical Engineering, BITS Pilani, Pilani Campus for providing the ATR−FTIR facility.

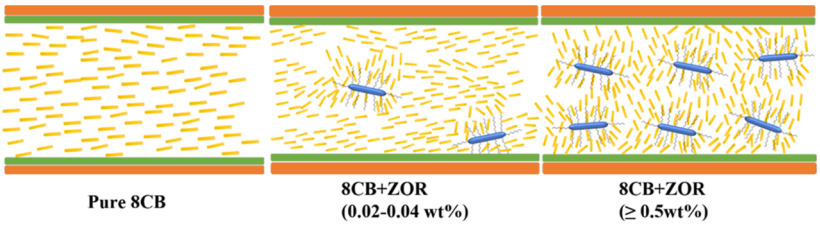

Figure 9. Schematic representation of VA of 8CB due to incorporation of ZOR.

https://doi.org/10.1021/acsomega.2c05196
ACS Omega 2022, 7, 46466−46474

REFERENCES

(1) SJ, S.; Gupta, R. K.; Kumar, S.; Manjuladevi, V. Enhanced Electro-Optical Response of Nematic Liquid Crystal Doped with Functionalised Silver Nanoparticles in Twisted Nematic Configuration. *Liq. Cryst.* **2020**, *47*, 1678−1690.

(2) Baik, I. S.; Jeon, S. Y.; Lee, S. H.; Park, K. A.; Jeong, S. H.; An, K. H.; Lee, Y. H. Electrical-Field Effect on Carbon Nanotubes in a Twisted Nematic Liquid Crystal Cell. *Appl. Phys. Lett.* **2005**, *87*, 263110.

(3) Kumar, P.; Jaggi, C.; Sharma, V.; Raina, K. K. Advancements of Vertically Aligned Liquid Crystal Displays. *Micron* **2016**, *81*, 34−47.

(4) Oh-e, M.; Yokoyama, H.; Kim, D. Mapping Molecular Conformation and Orientation of Polyimide Surfaces for Homeotropicliquid Crystal Alignment by Nonlinear Optical Spectroscopy. *Phys. Rev. E: Stat. Phys., Plasmas, Fluids, Relat. Interdiscip. Top.* **2004**, *69*, 11.

(5) Lee, S. H.; Lee, S. L.; Kim, H. Y. Electro-Optic Characteristics and Switching Principle of a Nematic Liquid Crystal Cell Controlled by Fringe-Field Switching. *Appl. Phys. Lett.* **1998**, *73*, 2881−2883.

(6) Shirota, K.; Yaginuma, M.; Sakai, T.; Ishikawa, K.; Takezoe, H.; Fukuda, A. Surface Orientation of Cyanobiphenyl Liquid Crystal Monolayer and Pretilt Angle under Various Rubbing Strengths. *Jpn. J. Appl. Phys.* **1996**, *35*, 2275−2279.

(7) Haba, O.; Hiratsuka, D.; Shiraiwa, T.; Funakoshi, N.; Awano, H.; Koda, T.; Takahashi, T.; Yonetake, K.; Kwak, M.; Momoi, Y.; Kim, N.; Hong, S.; Kang, D.; Choi, Y. Homeotropic Orientation of Nematic Liquid Crystals Induced by Dissolving Polypropyleneimine Dendrimer Having Peripheral Mesogens. *Opt. Mater. Express* **2014**, *4*, 934.

(8) van Aerle, N. A. J. M.; Barmentlo, M.; Hollering, R. W. J. Effect of rubbing on the molecular orientation within polyimide orienting layers of liquid-crystal displays. *J. Appl. Phys.* **1993**, *74*, 3111−3120.

(9) Lee, Y. J.; Kim, Y. W.; Ha, J. D.; Oh, J. M.; Yi, M. H. Synthesis and characterization of novel polyimides with 1-octadecyl side chains for liquid crystal alignment layers. *Polym. Adv. Technol.* **2007**, *18*, 226−234.

(10) Mishra, S.; Manjuladevi, V.; Gupta, R. K.; Kumar, S. Experimental Evidence of Continuous Isotropic-Nematic Phase Transition in CdS Nanowire Nanocomposites of a Nematic Liquid Crystal. *Liq. Cryst.* **2020**, *48*, 1151−1161.

(11) Moon, J.; Kang, C.; Kang, H. Vertical Alignment of Liquid Crystals on Phenylphenoxymethyl-Substituted Polystyrene-PS Derivatives Structurally Similar to LC Molecules. *Polymers* **2022**, *25*, 934.

(12) Sivaranjini, B.; Mangaiyarkarasi, R.; Ganesh, V.; Umadevi, S. Vertical Alignment of Liquid Crystals over a Functionalized Flexible Substrate. *Sci. Rep.* **2018**, *8*, 8891.

(13) Chen, S. H.; Chou, T. R.; Chiang, Y. T.; Chao, C. Y. Nanoparticle-Induced Vertical Alignment Liquid Crystal Cell with Highly Conductive PEDOT:PSS Films as Transparent Electrodes. *Mol. Cryst. Liq. Cryst.* **2017**, *646*, 107−115.

(14) Fang, G.; Shi, Y.; Maclennan, J. E.; Clark, N. A.; Farrow, M. J.; Walba, D. M. Photo-Reversible Liquid Crystal Alignment Using Azobenzene-Based Self-Assembled Monolayers: Comparison of the Bare Monolayer and Liquid Crystal Reorientation Dynamics. *Langmuir* **2010**, *26*, 17482−17488.

(15) Yi, Y.; Farrow, M. J.; Korblova, E.; Walba, D. M.; Furtak, T. E. High-Sensitivity Aminoazobenzene Chemisorbed Monolayers for Photoalignment of Liquid Crystals. *Langmuir* **2009**, *25*, 997−1003.

(16) Jeng, S. C.; Kuo, C. W.; Wang, H. L.; Liao, C. C. Nanoparticles-Induced Vertical Alignment in Liquid Crystal Cell. *Appl. Phys. Lett.* **2007**, *91*, 061112.

(17) Koenig, G. M.; Gettelfinger, B. T.; de Pablo, J. J.; Abbott, N. L. Using Localized Surface Plasmon Resonances to Probe the Nanoscopic Origins of Adsorbate-Driven Ordering Transitions of Liquid Crystals in Contact with Chemically Functionalized Gold Nanodots. *Nano Lett.* **2008**, *8*, 2362−2368.

(18) Qi, H.; Hegmann, T. Formation of Periodic Stripe Patterns in Nematic Liquid Crystals Doped with Functionalized Gold Nanoparticles. *J. Mater. Chem.* **2006**, *16*, 4197−4205.

(19) Zhao, D.; Zhou, W.; Cui, X.; Tian, Y.; Guo, L.; Yang, H. Alignment of Liquid Crystals Doped with Nickel Nanoparticles Containing Different Morphologies. *Adv. Mater.* **2011**, *23*, 5779−5784.

(20) Kinkead, B.; Hegmann, T. Effects of size, capping agent, and concentration of CdSe and CdTequantum dots doped into a nematic liquid crystal on the optical and electro-optic properties of the final colloidal liquid crystal mixture. *J. Mater. Chem.* **2010**, *20*, 448−458.

(21) Qi, H.; Hegmann, T. Liquid Crystal-Gold Nanoparticle Composites. *Liq. Cryst. Today* **2011**, *20*, 102−114.

(22) Kim, K. H.; Park, B. W.; Choi, S. W.; Lee, J. H.; Kim, H.; Shin, K. C.; Kim, H. S.; Yoon, T. H. Vertical Alignment of Liquid Crystals without Alignment Layers. *Liq. Cryst.* **2013**, *40*, 391−395.

(23) Hwang, S. J.; Jeng, S. C.; Yang, C. Y.; Kuo, C. W.; Liao, C. C. Characteristics of Nanoparticle-Doped Homeotropic Liquid Crystal Devices. *J. Phys. D Appl. Phys.* **2009**, *42*, 025102.

(24) Ma, H.; Lu, S.; Xie, Q.; Wang, T.; Lu, H.; Yu, L. A Stable Liquid Crystals Sensing Platform Decorated with Cationic Surfactant for Detecting Thrombin. *Microchem. J.* **2021**, *170*, 106698.

(25) Luan, C.; Luan, H.; Luo, D. Application and Technique of Liquid Crystal-Based Biosensors. *Micromachines* **2020**, *11*, 176.

(26) Sawamura, M.; Kawai, K.; Matsuo, Y.; Kanie, K.; Kato, T.; Nakamura, E. Stacking of Conical Molecules with a Fullerene Apex into Polar Columns in Crystals and Liquid Crystals. *Nature* **2002**, *419*, 702−705.

(27) Kuo, C. W.; Jeng, S. C.; Wang, H. L.; Liao, C. C. Application of Nanoparticle-Induced Vertical Alignment in Hybrid-Aligned Nematic Liquid Crystal Cell. *Appl. Phys. Lett.* **2007**, *91*, 141103.

(28) Goodby, J. W.; Saez, I. M.; Cowling, S. J.; Görtz, V.; Draper, M.; Hall, A. W.; Sia, S.; Cosquer, G.; Lee, S. E.; Raynes, E. P. Transmission and Amplification of Information and Properties in Nanostructured Liquid Crystals. *Angew. Chem., Int. Ed.* **2008**, *47*, 2754−2787.

(29) Li, Y.; Zhang, W. B.; Hsieh, I. F.; Zhang, G.; Cao, Y.; Li, X.; Wesdemiotis, C.; Lotz, B.; Xiong, H.; Cheng, S. Z. D. Breaking Symmetry toward Nonspherical Janus Particles Based on Polyhedral Oligomeric Silsesquioxanes: Molecular Design, "Click" Synthesis, and Hierarchical Structure. *J. Am. Chem. Soc.* **2011**, *133*, 10712−10715.

(30) Acharya, S.; Kundu, S.; Hill, J. P.; Richards, G. J.; Ariga, K. Nanorod-Driven Orientational Control of Liquid Crystal for Polarization-Tailored Electro-Optic Devices. *Adv. Mater.* **2009**, *21*, 989−993.

(31) Wu, K. J.; Chu, K. C.; Chao, C. Y.; Chen, Y. F.; Lai, C. W.; Kang, C. C.; Chen, C. Y.; Chou, P. T. CdS Nanorods Imbedded in Liquid Crystal Cells for Smart Optoelectronic Devices. *Nano Lett.* **2007**, *7*, 1908−1913.

(32) Acharya, S.; Panda, A. B.; Efrima, S.; Golan, Y. Polarization Properties and Switchable Assembly of Ultranarrow ZnSe Nanorods. *Adv. Mater.* **2007**, *19*, 1105−1108.

(33) Mishra, S.; Manjuladevi, V.; Gupta, R. K.; Kumar, S. Investigation on Physical Properties of Silver Nanorod Doped Nematic Liquid Crystal. *AIP Conf. Proc.* **2021**, *2369*, 020065.

(34) S J, S.J.; Mishra, S.; Dutta, K.; Gupta, R. K.; V, M. Frequency Dependence of Dielectric Permittivity and Conductivity of Functionalized Carbon Nanotube-Nematic Liquid Crystal Nanocomposite. *J. Mol. Liq.* **2022**, *349*, 118168.

(35) Singh, D.; Singh, U. B.; Pandey, M. B.; Dabrowski, R.; Dhar, R. Enhancement in Electro-Optical Parameters of Nematic Liquid Crystalline Material with SWCNTs. *Opt. Mater.* **2018**, *84*, 16−21.

(36) Basu, R.; Atwood, L. J. Homeotropic liquid crystal device employing vertically aligned carbon nanotube arrays as the alignment agent. *Phys. Rev. E* **2020**, *102*, 22701.

(37) Yin, M.; Gu, Y.; Kuskovsky, I. L.; Andelman, T.; Zhu, Y.; Neumark, G. F.; O'Brien, S. Zinc Oxide Quantum Rods. *J. Am. Chem. Soc.* **2004**, *126*, 6206−6207.

(38) Li, C.; Li, Y.; Wu, Y.; Ong, B. S.; Loutfy, R. O. Synthesis of Zinc Oxide Nanocrystals by Thermal Decomposition of Zn-Oleate in Organic Medium. *Sci. China, Ser. E: Technol. Sci.* **2008**, *51*, 2075−2079.

https://doi.org/10.1021/acsomega.2c05196
ACS Omega 2022, 7, 46466−46474

(39) Urbanski, M. On the Impact of Nanoparticle Doping on the Electro-Optic Response of Nematic Hosts. *Liq. Cryst. Today* **2015**, *24*, 102−115.
(40) Su, H.; Zhang, J.; Wang, C.; Wang, Y.; Zhao, H. Vertical Alignment of Liquid-Crystal Molecules Due to Unilateral Anchoring from Charge Accumulation at the Semiconductor Interface. *Rev. Phys. Appl.* **2019**, *12*, 1.
(41) Urbanski, M.; Mirzaei, J.; Hegmann, T.; Kitzerow, H. S. Nanoparticle Doping in Nematic Liquid Crystals: Distinction between Surface and Bulk Effects by Numerical Simulations. *ChemPhysChem* **2014**, *15*, 1395−140.
(42) Cseh, L.; Mehl, G. H. Structure-Property Relationships in Nematic Gold Nanoparticles. *J. Mater. Chem.* **2007**, *17*, 311−315.
(43) Kumar, J.*Effect of Nanomaterial Dopants on the Physical Properties of Liquid Crystals*; Birla Institute of Technology and Science, 2016.
(44) Chinky; Kumar, P.; Sharma, V.; Malik, P.; Raina, K. K. Nano Particles Induced Vertical Alignment of Liquid Crystal for Display Devices with Augmented Morphological and Electro-Optical Characteristics. *J. Mol. Struct.* **2019**, *1196*, 866−873.
(45) Choudhary, A.; George, T. F.; Li, G.Theoretical Analysis of Nanoparticle-Induced Homeotropic Alignment in Nematic Liquid Crystals. **2015**, arXiv:1510.08166.
(46) Singh, D. P.; Gupta, S. K.; Yadav, S. P.; Sharma, P. K.; Pandey, A. C.; Manohar, R. Guest-host interaction in ferroelectric liquid crystal-nanoparticle composite system. *Bull. Mater. Sci* **2014**, *37*, 511−518.
(47) Garbovskiy, Y. Kinetics of Ion-Capturing/Ion-Releasing Processes in Liquid Crystal Devices Utilizing Contaminated Nanoparticles and Alignment Films. *Nanomaterials* **2018**, *8*, 59.
(48) Lebovka, N.; Dadakova, T.; Lysetskiy, L.; Melezhyk, O.; Puchkovska, G.; Gavrilko, T.; Baran, J.; Drozd, M. Phase Transitions, Intermolecular Interactions and Electrical Conductivity Behavior in Carbon Multiwalled Nanotubes/Nematic Liquid Crystal Composites. *J. Mol. Struct.* **2008**, *887*, 135−143.
(49) Singh, D. P.; Duponchel, B.; Lin, Y.; Blach, J. F.; Khemakhem, H.; Legrand, C.; Douali, R. Orientation of 4-n-octyl-4′-cyanobiphenyl molecules on graphene oxide surface via electron-phonon interaction and its applications in nonlinear electronics. *J. Mater. Chem. C* **2019**, *7*, 2734−2743.
(50) Hayashi, S.; Kurita, K.; Kimura, N.; Umemura, J.; Takena, T. FT-IR Studies on Molecular Structure and Orientation of a Liquid Crystal, 4'-n-Octyl-4-Cyanobiphenyl. *Bull. Inst. Chem. Res.* **1985**, *63*, 276−295.
(51) Smela, E.; Martínez-miranda, L. J. X-Ray Study of Liquid Crystal Alignment: Evidence for an Alternate Mesophase at the Free Surface? *Mol. Cryst. Liq. Cryst.* **1991**, *203*, 1−8.
(52) Schweicher, G.; Gbabode, G.; Quist, F.; Debever, O.; Dumont, N.; Sergeyev, S.; Geerts, Y. H. Homeotropic and Planar Alignment of Discotic Liquid Crystals: The Role of the Columnar Mesophase. *Chem. Mater.* **2009**, *21*, 5867−5874.
(53) Van Aerle, N. A. J. M. Anchoring of 4-n-alkyl-4′-cyanobiphenyl liquid crystal molecules on rubbed polyimides. *Liq. Cryst.* **1994**, *17*, 585−588.

https://doi.org/10.1021/acsomega.2c05196
ACS Omega 2022, 7, 46466−46474